The Institute of Space and Astronautical Science
Report SP No. 15, March 2003

Leonid at 1000 frames per second

By

Hans. C. STENBAEK-NIELSEN* and Peter JENNISKENS†

(1 February 2003)

Abstract: At 10:42:59 UT, 18 November 2001, a -3 magnitude Leonid meteor was recorded with an intensified CCD imager at 1000 frames per second. The observation was made at Poker Flat Research Range north of Fairbanks, Alaska. The high-speed imager covered the main brightening phase as the Leonid descended from an altitude of 115.6 km to 104.4 km. With millisecond resolution there is no "smearing" due to meteor motion. Below 111 km a large, several 100 m wide, shock-like structure developed. Such structure has not previously been reported. The size is surprisingly large and cannot be explained by classical fluid dynamics. We speculate that additional processes driven by intense UV radiation from the heated meteor core leading to photo ionization of the ambient air may play an important role.

1. INTRODUCTION

Our current understanding of how meteors deposit material in the atmosphere and change its chemical composition is mostly based on spatially unresolved optical and radar observations, which cannot provide detailed information about the processes involved. Further, the physical characteristics of meteors are complicated by fragmentation of the meteoroid, the formation of a vapor cloud of molecules and atoms sputtered off the meteoroid, fragments ejected at high speed from a spinning grain, and non-equilibrium chemistry in the meteor wake. For an extensive review of meteors see Ceplecha et al. (1998). In order to understand the physical processes, it would be most helpful to resolve the morphological features. Here, we present the first high frame-rate (1000/s) imaging of a -3 magnitude Leonid meteor that was captured during the 2001 Leonid meteor storm as part of the larger Leonid Multi-Instrument Aircraft Campaign (Jenniskens and Butow 1999) targeted to the 2001 Leonid meteor storms. The images show the development of a large, shock like structure in front of the meteor and a region that appears to be a zone of pre-dissociation and pre-ionization.

2. INSTRUMENTATION

The observations were made at the University of Alaska's Poker Flat research Range 30 miles northeast of Fairbanks, Alaska (65.12N, 147.46W, and 0.39 km altitude) with an intensified

* Geophysical Institute, University of Alaska, Fairbanks, Alaska, USA.
† SETI Institute, 2035 Landings Drive, Mountain View, CA 94043, USA.

CCD camera operating at 1000 frames per second (fps). The CCD images are 256×256 pixels with 256 gray levels (8 bits) and $6.4° \times 6.4°$ field of view. At 1000 fps gray level 255 is reached at 3 MR (at 700 nm), which is about 25% CCD well depth. The intensifier is sensitive to light in the wavelength range 500 - 900 nm with peak sensitivity at 700 nm. The gain is affected by total scene brightness in a way that is not easy to quantify. The intensifier phosphor has a decay time constant of 0.8 ms, and hence some "afterglow" may be discernible for a few frames following targets with rapid spatial or temporal variations. However, it does not appear that either potential problems affects the observations.

The high-speed imager was bore sighted with a wide field low light level TV system. This system is also an intensified CCD, and the data are recorded on videotape with standard NTSC resolution (60 interlaced fields per second) and with GPS time encoded. The field of view is $21° \times 16°$, and the intensifier responds to light in the wavelength range of 400–800 nm.

The basic sensitivity of the two imaging systems is fairly similar, but with 1 ms time resolution for the high speed imager versus 30 ms for the TV system a corresponding difference in effective sensitivity is introduced. At 1000 fps the high speed imager is measured to saturate (pixel value 255) at 3 MR, while the TV system saturates at 50 kR. Thus the TV system would provide the best data at light levels, which the high speed imager would record at very low signal to noise levels.

3. DATA

On the night of November 18 UT, 2001, the weather was mostly clouded. After 10 UT the eastern sky cleared and at 10:42:59 UT, close to the peak of the Leonid storm at ~10:40 UT caused by Earth's crossing of the 1767 dust trail of comet 55P/Tempel-Tuttle, a bright Leonid meteor passed through the field of view of both imagers. 463 images were recorded of the meteor at 1000 frames per second.

Figure 1 shows representative frames from the high-speed imager sequence of this event. Each image is a $0.94° \times 0.94°$ section of the original $6.4° \times 6.4°$ images centered on the meteor. The meteor enters the field of view at near frame 60 within the sequence. The meteor is initially a point source, saturated at the center and slightly broader than the unsaturated star images, with only a faint trace of wake. However, around frame 235 a distinct spatial structure reminiscent of a shock develops. The emission on the outside of the "shock" structure gradually brightens forming a circle of light with a piece cut out. At the same time the "shock" opens up. The structure reaches is maximum size near frame 330, which is also the time of maximum meteor brightness. This is the first time that such spatial structure has been reported.

The spatial structure is not the result of optical reflections in the camera. We note that the images are already distinctly asymmetric when the meteor passes very close to the optical axis of the camera (frame 300), where any instrumental effects are expected to be symmetric. The blooming of the brightest part remains modest throughout the exposure period, and is much less than the observed spatial structure. The diffuse glow, much wider than any spatial structure in the images, is probably due to scattering of light in the thin clouds present.

The meteor moves, on average, 0.6 pixels between successive images. Thus there is no "smearing" of structure due to the motion of the meteor. The pixel size in the high-speed images is $0.025° \times 0.025°$. At a range of 135 km, corresponding to an altitude of about 110 km, the spatial resolution would be 57 m. The radiant for the shower is at $154.1° \pm 0.2°$ right ascension and $21.4° \pm 0.1°$ declination, and the entry velocity is 71.6 ± 0.4 km/s (Betlem et al. 1999). At the time of the event, 10:42:59 UT, the radiant was at 86.5° azimuth (East of North) and 22.3°

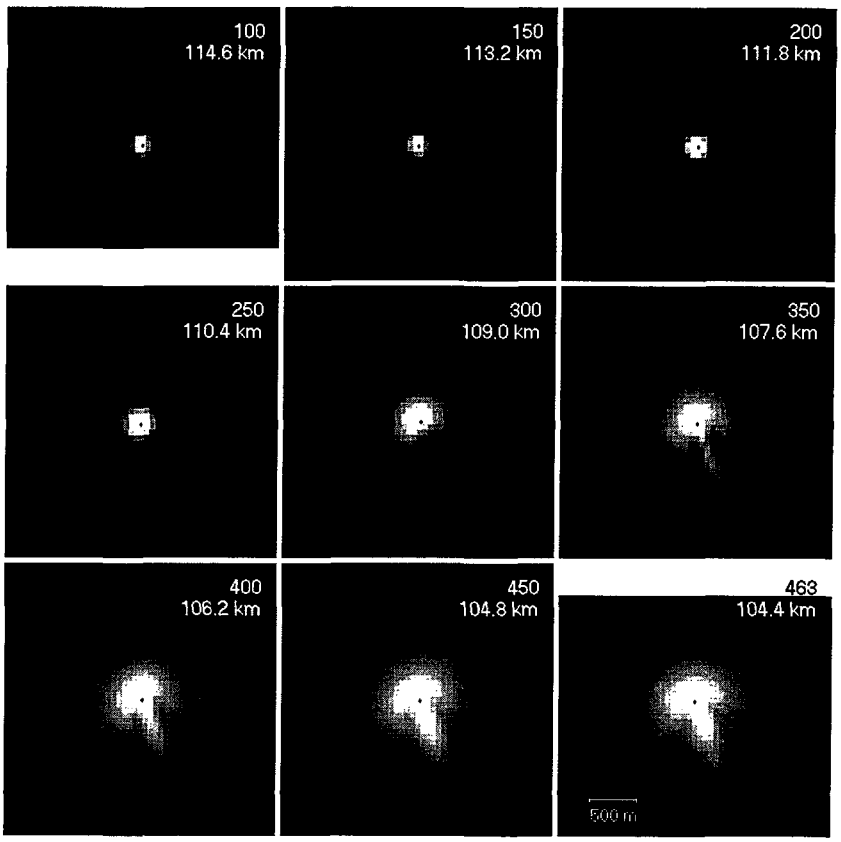

Fig. 1: Selected frames from the high-speed imager. Each image is a 1 ms exposure. The fitted meteor position is shown, and frame number and altitude are given in the upper right corner.

elevation. The camera orientation was 76.1° azimuth and 53.9° elevation resulting in an angle between camera orientation and the meteor velocity vector varying from 28° to 33° across the field of view. Thus structures along the meteor trajectory in the images will be foreshortened by roughly a factor of 2 and the spatial resolution along the trajectory would be 114 m.

The event was also recorded with the co-aligned wide field intensified CCD TV imager. Figure 2 shows four frames from the video. The field of view is 21° × 16° and the High Speed Imager covers the central 6.4° × 6.4°. The TV frames show clear evidence of "smearing" due to meteor motion. Also, saturation cause the detector to "bloom". These effects combine to make it impossible to resolve any of the structures within the head of the meteor. The meteor passed from the bottom to the top across the central part of the images in a little less than 1 second. The first image in figure 3 shows the meteor just before it enters and the last just after it exits the HSI field of view. Note that the peak luminosity of the meteor is reached at the top center of the field of view. Thus the rise to peak luminosity is covered by the High Speed Imager. The luminosity falls off rapidly as the meteor exits the TV field of view. The TV images show the wake that remains in the path of the meteor. The brightness of the wake mimics the variation of brightness around the peak and it remains visible for about 2 s.

The TV images show the presence of haze or thin clouds. The haze is not uniform across the field of view. The limiting stellar magnitude in the images is slightly less than 7. For ground based observations at maximum instrument gain and with a dark, clear sky we would

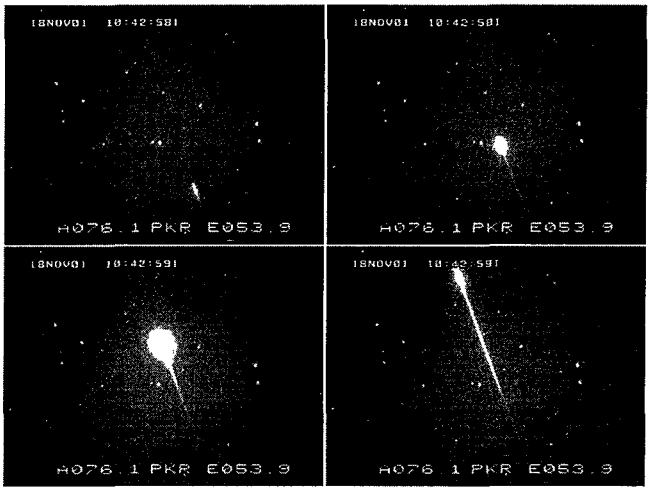

Fig. 2: Four fields from the video camera showing the time development of the meteor. The field of view is 21 × 16 degrees, and the high-speed imager the central 6.4 × 6.4 degrees.

expect to see stars down to magnitude 8.5. Based on the light curve extracted from the TV record the magnitude of the meteor is -2.7 ± 0.5.

4. ANALYSIS AND DISCUSSION

The high-speed images and the wide-field images have been analyzed to provide information about the time development of various features such as relative brightening, altitude, and the development of the shock-like structure. The track across the field of view together with orbital information about the Leonids can provide the altitude of the meteor.

4.1 Meteor path

Direction to features in the HSI and TV images is based on the stars visible in the images. Both data sets have a sufficient number of stars distributed across the images to allow good spatial calibration. Using computer routines developed for analysis of image data in connection with auroral research (Stenbaek-Nielsen et al. 1984) stars in the Smithsonian Astronomical Observatory star catalog are overlaid and fitted to the stars present in the images. The fitting program is interactive and can accommodate non-linearities in the display. The resulting star fit provides directional information to all pixels within the individual images.

The center location of the meteor in each image was measured for all images in both the HSI and the video data sequences. A computer program was written to calculate the location of the meteor in each image within the two image sequences using a fixed meteor velocity vector and an initial starting point. The velocity vector is given by the Leonid orbital parameters (Betlem et al. 1999) resulting in a radiant position of $154.1° \pm 0.2°$ right ascension and $21.4° \pm 0.1°$ declination. The velocity is 71.6±0.4 km/s, which is sufficiently high that changes due to the Earth's gravitational field may be neglected. The starting point was derived from the meteor location in one of the early HSI images. Here the angle to the meteor is well defined, and with an assumed range an initial geographic position can be defined and subsequent positions calculated. The calculated positions were compared to the observed and the initial

parameters (velocity vector and initial range) were adjusted for an overall best fit.

The best-fit was obtained by adjusting the assumed range to the initial point and the Leonid velocity vector. The fit show no indication of a change in velocity over the period of observations in agreement with Spurny et al. (2000), who reported that the deceleration of similar Leonid meteors was below measurement accuracy. At the time of the event, 10:42:59 UT, the direction of the meteor track in the images is most sensitive to the value of the right ascension. A good fit to the observation was obtained for a right ascension of 154.0° and a declination of 21.6°. This is within the range given by Betlem et al. (1999). The motion along the track in the images will depend on the meteor velocity, the assumed range to the selected initial point, and, to a lesser degree, the declination of the radiant. We have assumed a Leonid velocity of 71.6 km/s and then adjusted the range to the initial point to obtain a best fit between calculated and observed positions. But varying the assumed range to the initial point can compensate for any reasonable change in the Leonid velocity. Thus the analysis is essentially insensitive to smaller variations in the Leonid velocity.

4.2 Meteor altitude

The track fitted to the observed locations of the meteor across the field of view provides the altitude of the meteor. The fitted altitudes are given with the images presented. As mentioned above, the fitting procedure is not very sensitive to changes in Leonid entry velocity; if the velocity decreases by 1 km, the derived altitudes would decrease by 2 km. The meteor entered the wide field of view camera at an altitude of 128.1 km and the HSI field of view at 115.6 km. The shock structure started to develop at 110.4 km and was fully developed at 106 km, when the meteor brightness leveled off. The video images show a fairly broad maximum in luminosity centered at an altitude of 103 km, after which the meteor decreased in intensity. It left the wide field of view camera at an altitude of 96.3 km, still at magnitude +1, but fading rapidly, and the video camera would not have detected the meteor much beyond this point. The derived altitudes are in good agreement with altitudes found for similar Leonid meteors (Jenniskens 1999; Betlem et al. 1999; DeLignie et al. 2000).

4.3 Relative brightness

The meteor brightens substantially during the time it moves across the 6.4° × 6.4° field of view of the high-speed imager. Figure 3 shows the signal integrated across a 41 × 41 pixel area centered on the meteor. The central sections of the meteor in the images are clearly saturated throughout the image sequence. Since the intensifier and CCD are designed to minimize saturation effects ("blooming") the saturated pixels in the images would be contributing relatively less to the integrated brightness, and therefore, the derived brightness would be an underestimate.

The relative brightness increases slowly until frame 230 when a rapid increase starts. It is during this increase we see spatial structure develop (figure 1). The brightness increase levels off after frame 360. The subsequent increase after frame 420 seems to be associated with a broad, general increase in luminosity in the section to the right of the meteor. This 20% increase is not present in the TV images and may reflect the different ways the two imagers handles saturation. While the TV responds with "blooming", which will essentially preserve the total signal, the high-speed imager is designed to minimize saturation effects. This could imply that the increase in the high speed data is due to a redistribution of optical emissions from

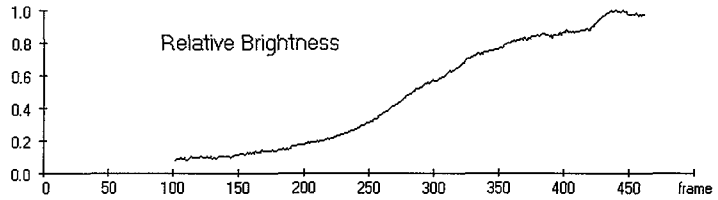

Fig. 3: Total brightness of the meteor derived from the high-speed images.

the saturated central region of the meteor (where light above saturation will not be registered by the high-speed imager) to the "glow" outside that region. This would be consistent with scattering in a locally varying thin cloud layer.

4.4 Observed wake

In the wake of the meteor there is first a rapid decay of light, meteor afterglow, from collisional excitation o metal atoms and air plasma compounds (Halliday 1958). This is best seen in the meteor around frame 350-400. The decay 1/e time is 4.7 ms significantly above the phosphor decay time of 0.8 ms. This time scale may be associated with the formation of the meteor plasma wake, which would thus stretch to a typical 1/e length scale of 4.7 ms $\times$ 71.6 km/s = 340 m. Then with small delay the long tail forms (figure 2) with emissions primarily from the forbidden OI transition at 557.7 nm (Baggalay 1976). The conditions in the region of the wake are important for the possible deposition of organic material from the meteoroid to the atmosphere. A more detailed evaluation of this aspect of the observation, including a more detailed brightness evaluation, may be found in Jenniskens and Stenbaek-Nielsen (2002).

4.5 The bow shock

Perhaps the most significant observation is the formation of a large, shock like structure as the meteor enters the atmosphere. This feature has not been reported before. In Figure 1 the development is seen from frame 250 on. Behind the meteor there is a significant reduction in emissions on both sides of the tail. The dimension across this region is $\sim$500 m.

The structure clearly shows some curvature and a parabola fits the observations very well. For the purpose of analysis, we will assume the shock like structure to be a sheath in the shape of a paraboloid with the meteor body at the focal point. Because of the 30° angle between the meteor trajectory and our line of sight, the front of the parabola in the images is not at the front of the paraboloid, but at a tangent point off to the side. Therefore the observed distance from the focal point (the meteor) would be larger than the actual focal distance for the paraboloid. The necessary correction can easily be derived through simple geometrical considerations. For a 30° angle to the trajectory, the focal distance will be 3/4 of the distance inferred from the image. For the analysis we fitted to the "inner" edge, which is relatively easy to identify consistently throughout the data set. Figure 4 shows the fit for four individual frames. The parabola clearly is opening up as the structure develops.

Before going farther with the analysis, it must be kept in mind that our observations are 2-D projections of a 3-D object. While it appears very reasonable to assume a paraboloid with rotational symmetry, the projection at a 30° angle to the line of sight may introduce asymmetries into the images not adequately represented by the assumed resulting shape of a

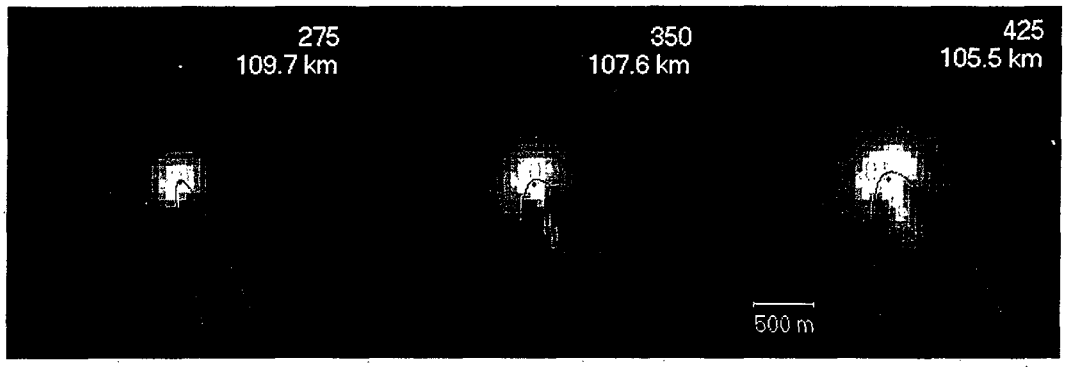

Fig. 4: Parabola fitted to shock structure. The size of the structure is seen to increase with time.

parabola. The images represent line-of-sight integrated brightness through a 3-D object and a more detailed modeling of the object may provide additional insight into the nature of the structure observed.

Figure 5 gives the variation in focal distance for the data set. The focal distance is seen to increase from a few meters to about 40 meters at frame 400 after which it levels off. Frame 400 is approximately the time of maximum brightness of the meteor. After this the shock becomes less well defined. The subsequent decrease in brightness is clearly evident in the video images (figure 2). The focal distances are unexpectedly large compared with the estimated 2 m total size of the ablation cloud for such a meteor (Boyd 2000) and would be difficult to explain by classical fluid dynamics. Hence, what is the cause?

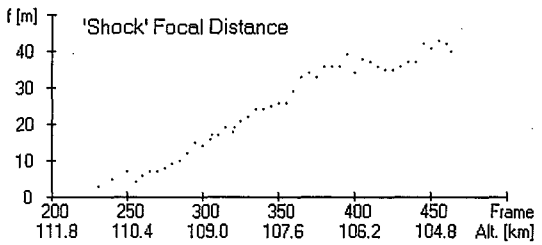

Fig. 5: Inferred focal distance for the shock as function of time and altitude

An obvious line of inquiry would be the role of ionization. Meteor spectra show the presence of metallic ions (Borovicka et al. 1999), but oxygen and nitrogen ions have not been reported. At 71 km/s molecules and atoms would have substantial kinetic energy and collisions with the ambient atmosphere should lead to optical emissions as well as ionization. In this context it is rather surprising that no ionized oxygen or nitrogen ion emissions are seen. If there are a significant number of ions in the Leonid ablation cloud interaction with the Earth's magnetic field will set up a polarization field (positive changes ions and electrons will be deflected in opposite directions). The magnitude of the polarization field would be 3.5 V/m (determined by the 71.6 km/s meteor velocity and a magnetic field strength of 50000 nT to give an ExB drift of 71.6 km/s). But at 100 km altitude the ion mean free path is only 1 m, and it is difficult to envision processes leading to the very large observed structure.

A more promising line of inquiry may be ionization and emissions due to UV radiation from

the meteor, which may reach a temperature of 4400K (Borovicka et al. 1999). Indeed, most of the emitted light outside of the bow shock may originate from ionization and dissociation of the ambient air caused by UV photons emitted from the bow shock or the meteor plasma. The 1/e penetration depth of UV photons of ~8eV generated in a shock is about 22 m at 89 km (Zinn J. et al. 1999), which translates to 304 m at 105 km, where our feature is seen. The diameter of the sphere-like feature that makes up most of the light emission is about 380±50 m, in good agreement.

The saturation of the images prevents a direct determination of the relative importance of emission from the bow shock and from the immediate region of the meteor. However, in addition to shock and wake, there is a diffuse halo surrounding the meteor image that is of such large dimension that it can only be due to scattering of light. The halo has a Gaussian distribution of light, with the center of the emission less than 1 pixel from the position of the meteor, not on the shock. This is further evidence that the bulk of the light originates from very close to the meteoroid position and not from the shock.

5. CONCLUSIONS

High-speed imaging has revealed previously unseen spatial structure in bright meteors. Details are seen in the formation of the wake that allowing a critical evaluation of possible deposition into the Earth's atmosphere of organic molecules carried by the meteor. The scale size of the discovered bow-shock like structure is large, several 100 m, which cannot be explained by classical fluid dynamics. We suggest that the structure is likely associated with photo ionization processes driven by intense UV radiation from the meteor and its ablation cloud frictionally heated to 4400K. Observations from the planned 2002 Leonid MAC mission may aid considerably in the development of a better understanding of the physics of Leonid meteors.

ACKNOWLEDGMENTS

We thank the Astrobiology program for support of the Leonid MAC program. This paper was partially supported by the International Symposium Grant of the Japanese Ministry of Education, Culture, Sports, Science and Technology (MEXT) and the Institute of Space and Astronautical Science (ISAS), Japan.

REFERENCES

Baggalay W. J., Bull. Astron. Inst. Czechoslov., 27, 173–181, 1976.
Betlem H., et al. Meteoritics and Planetary Science 34, 979–986, 1999.
Borovicka J., Stork R., Bocek J., Meteorit. Planet. Sci. 34, 987–994, 1999.
Boyd, I. D., Earth, Moon and Planets 82–83, 93–108, 2000.
Ceplecha Z., et al. Space Science Reviews, 84, 327–471, 1998.
DeLignie, M., et al. Earth, Moon and Planets 82–83, 295–304, 2000.
Halliday I., Astrophysical Journal, 127, 245–252, 1958.
Jenniskens P., Meteoritics and Planetary Science 34, 959–968, 1999.
Jenniskens P., Stenbaek-Nielsen, H. C., Astrobiology, submitted, 2002.
Jenniskens, P., Butow, S.J., Meteoritics Planet. Sci., 34, 933–943, 1999.
Spurny, P., Betlem, H., Van t' Leven, J., Jenniskens, P., Meteoritic. Planet. Sci., 35, 243–249, 2000.
Stenbaek-Nielsen H.C., Hallinan T. J., Wescott E. M., Fppl H., J. Geophys. Res., 89, 10788–10800, 1984.
Zinn J., et al. Meteorit. and Plan. Sci. 34, 1007–1015, 1999.